LONG-TERM SEISMIC RISK ASSESSMENT CONSIDERING THE TRIGGERED AFTERSHOCKS

Conference Paper · June 2019

DOI: 10.7712/120119.7104.19740

2 authors:

F. Jalayer
University of Naples Federico II

Hossein Ebrahimian
University of Naples Federico II

COMPDYN 2019
7th ECCOMAS Thematic Conference on
Computational Methods in Structural Dynamics and Earthquake Engineering
M. Papadrakakis, M. Fragiadakis (eds.)
Crete, Greece, 24–26 June 2019

LONG-TERM SEISMIC RISK ASSESSMENT CONSIDERING THE TRIGGERED AFTERSHOCKS

Fatemeh Jalayer[1], **Hossein Ebrahimian**[2]

[1] Associate Professor
Department of Structures for Engineering and Architecture, University of Naples Federico II, Via Claudio 21, Naples 80125, Italy
e-mail: fatemeh.jalayer@unina.it

[2] Assistant Professor
Department of Structures for Engineering and Architecture, University of Naples Federico II, Via Claudio 21, Naples 80125, Italy
e-mail: ebrahimian.hossein@unina.it

Abstract

Assessment of the long-term risk profile considering the triggered seismic sequence is rendered complicated by the short-term clustering of aftershock events following the main event and the increased potential for damage accumulation. The assessment of long-term seismic risk profile for the main seismic events is based on the renewal of the structure to a prescribed state after each seismic event. In the case of a triggered aftershock sequence, it is very unlikely that the structure is repaired back to its intact condition during early phases of an ongoing sequence. Therefore, considering the (magnifying) effect of cumulative damage due to the triggered aftershock sequence in long-term seismic risk profile is not a trivial task. One viable strategy is to evaluate the increase in the (time-invariant) limit state excursion probability due to the combined effect of short-term aftershock clustering and the resulting cumulative damage for a prescribed post-event short-term time interval. As expected, in case the structure is assumed to be renewed to a given hypothetic damage state (such as main-shock damaged) after each event occurs, the formulation for limit state probability simplifies to a closed-form Poissonian formulation. The methodology is applied to an existing 3-story RC moment-resisting frame in central Italy. The Poissonian closed-form solution, with the hypothesis of renewal back to the main-shock damaged configuration, is shown to successfully capture the increase in the limit state probability due to the effect of the triggered sequence.

Keywords: Performance-based seismic assessment, Time-dependent reliability, Aftershock sequence, Cumulative damage, Non-linear dynamic analysis, Cloud Analysis.

1 INTRODUCTION

The damage-inducing potential of the aftershocks (AS) following the main event (mainshock, MS) is not considered explicitly in standard seismic risk assessment procedures. The guideline of advanced seismic assessment [1] provides a step-by-step procedure for estimating the fragility curves for a MS-damaged structure based on performance levels ranging from onset of damage to collapse. The seismic behavior of the MS-damaged structure is estimated by performing non-linear static analysis (pushover) on the damaged structure. The residual capacity of the MS-damaged structure is also estimated dynamically by subjecting the structure to a suite of back-to-back ground motion time histories (basically mimicking the effect of a mainshock and one severe aftershock) [2-4]. The use of back-to-back MS events (or their amplitude-scaled versions) as a proxy for the seismic sequence gives way to discussions on its adequacy for representing the frequency content and other ground motion characteristics of the aftershocks triggered by a strong earthquake [5-8]. One important message is that the back-to-back method may overestimate the damaging potential of the earthquakes with respect to when real seismic sequences are used. The demands induced by a sequence of as-recorded seismic events are investigated in [8-11]. Generating artificial MS-AS sequences are also devised in [12-13] paying attention to the frequency content of aftershocks.

Another issue that has received attention from the research community with regard to the aftershocks is the choice of the nonlinear dynamic analysis method for estimating the aftershock vulnerability. Most of the methods available in literature rely on incremental dynamic analysis (IDA, [14]) for calculating the residual capacity of the MS-damaged structure (see e.g., [2-4, 6, 15]). There are also methods in literature that use the so-called Cloud Analysis CA [16-18] for the prediction of the cumulative damage due to the aftershocks ([5, 10, 11, 19, 20]). CA employs linear logarithmic regression in order to predict the structural response versus the ground motion intensity measure based on as-recorded ground motions.

The evaluation of damaging potential of an AS sequence is a time- and history-dependent problem: the time-dependent decay in short- to medium-term seismicity and the history-dependent nature of structural behaviour in the nonlinear range. Quite a few works focus on tackling the problem of aftershock risk assessment considering this time- and history-dependence (see e.g., [4, 10, 11, 19]). Jalayer et al. [19] propose a method for calculating the limit state probability due to an AS sequence in an interval of time by using the total probability theorem. The methodology considers the uncertainty in the number of events of interest and the progressive damage induced by the occurrence of a sequence of aftershocks assuming independence between limit state exceedance in successive events. The method proposed in [19] has been refined in [10, 11] by considering the memory-dependence in calculating the limit state first-excursion due to successive AS records. The current work presents formal procedure for limit state probability assessment considering the MS and the triggered sequence of AS (MS+AS sequence) in contrast to risk calculated by only considering the strong motion (MS). This procedure, referred to as "*best-estimate*", considers explicitly both the time-dependent rate of occurrence for AS and the cumulative damage caused by the triggered seismic sequence (MS+AS sequence). Moreover, it is shown that, the implementation of an (time- and event-) invariant fragility curve in the formulation employed for calculating the limit state probabilities due to the triggered sequence [10], leads to the same simple Poisson-type functional form adopted when the cumulative damage is not considered (assuming that the structure's state is always "renewed" to the same initial state right after the event occurs) [11]. This, apart from verifying the formulation in a special and limiting case, provides the possibility of exploring alternative approximate and simplified solutions by adopting fragility curves corresponding to various initial conditions; such as, fragility curve for the intact structure, fragility curve for the MS-damaged structure, fragility curve for MS-plus-one-AS-damaged structure, and so on. It is particularly interesting to study the case of fragility curve for the MS-damaged structure since it (with some variations) is often used as a proxy for modeling the damage accumulation due to the MS+AS sequence.

As a numerical example, time-dependent risk related to MS+AS sequence is calculated through both the outlined "best-estimate" and "*approximate*" procedures. The numerical example herein uses a modified version of the sequential Cloud Analysis (CA) method [10, 11] considering explicitly the "collapse" cases, based on both back-to-back strong-motion (MS) records and also AS ground-motion records. Moreover, the sequential CA presented herein includes an embedded strategy in order to ensure that CA-based predictions do not involve extrapolations. Risk is evaluated in terms of the probability of exceeding the near-collapse limit state for a typical 3-story reinforced concrete (RC) frame building with infill panels located in L'Aquila, central Italy.

2 METHODOLOGY

To calculate the limit state exceedance probability due to a MS and the triggered AS sequence (MS+AS sequence), let P(τ)=$P(LS|\mathbf{I}_1)$ be the probability of the first-excursion of a desired limit state LS given the information $\mathbf{I}_1$ about MS+AS sequence as shown in Figure 1. The MS with magnitude $M_l \le M_{ms} \le M_u$ (M_l and M_u are the site-specific lower- and upper-bound magnitudes) is followed by an AS sequence with magnitudes M_{as} in the range $M_{l,as} \le M_{as} \le M_u$ ($M_{l,as}$ is the lower bound magnitude for AS) in the time interval [t_{ms},$t_{ms}+\tau$]; t_{ms} is the time of occurrence of the MS and τ is a given forecasting interval for the triggered aftershocks.

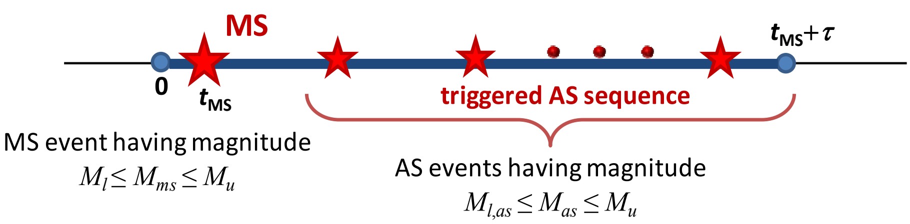

Figure 1: Information $\mathbf{I}_1$ about MS+AS sequence.

The probability P(τ) can be further broken down as follows: LS is exceeded due to the MS with the probability P_{ms}, or it is exceeded with probability $\mathrm{P}_{as}(\tau)$ during the AS sequence given that it is not exceeded due to the MS [11]:

$$\mathrm{P}(\tau) = \mathrm{P}_{ms} + p_{tr} \cdot (1 - \mathrm{P}_{ms}) \cdot \mathrm{P}_{as}(\tau) \quad (1)$$

The probability of exceeding the limit state LS in time interval [0, t], denoted as $P(LS)$ herein, can be expressed as (assuming a homogeneous Poisson stochastic model):

$$P(LS) = 1 - \exp\left(-\nu_{ms} \cdot \mathrm{P}(\tau) \cdot t\right) = 1 - \exp\left[-\nu_{ms} t \cdot \left(\mathrm{P}_{ms} + (1 - \mathrm{P}_{ms}) \cdot \mathrm{P}_{as}(\tau)\right)\right] \quad (2)$$

where ν_{ms} is the rate of occurrence of a MS with $M_l \le M_{ms} \le M_u$. It is assumed that each time a MS occurs, it hits the intact structure. Fitting a (filtered) homogeneous Poisson model herein implies that limit state first-excursion due to MS+AS sequence is lumped at the time of occurrence of the MS, t_{ms}; this is a reasonable assumption when τ is more than an order of magnitude smaller than t.

Adopting the first-mode spectral acceleration at period T, $Sa(T)$, as the desired ground motion intensity measure, P_{ms} in Eq. (1) or Eq. (2) can be calculated as:

$$\mathrm{P}_{ms} = 1/\nu_{ms} \int\limits_{\forall sa_{ms}} \pi_0\left(sa_{ms}\right) \cdot \left|\mathrm{d}\lambda_{ms}(sa_{ms})\right| \tag{3}$$

where sa_{ms} is $Sa(T)$ associated with the MS event; $\pi_0=P(LS_{ms}|sa_{ms})$ is the conditional probability of LS first-excursion for the MS event (a.k.a. the fragility of the intact structure); λ_{ms} is the site-specific hazard defined as the mean rate of exceeding $Sa(T)$ (note that the rate λ_{ms} and time t should have consistent units).

The probability P_{as} (the dependence on τ is dropped for brevity) is the limit state first-excursion probability associated with the AS sequence following the MS event given that the MS has not caused the limit state excursion. This term can be expanded based on Total Probability Theorem over all possible MS wave forms [11]:

$$\mathrm{P}_{as} = \int\limits_{\Omega_{MS}} P\left(LS_{as} \mid MS\right) p\left(MS\right) \mathrm{d}MS \approx 1/N \sum_{MS_i} P\left(LS_{as} \mid MS_i\right) \tag{4}$$

where $P(LS_{as}|MS)$ is the probability of LS first-excursion for an arbitrary AS event belonging to the AS sequence, given a MS (note that knowing the MS means that its waveform and other characteristics such as intensity are known); $p(MS)$ is the probability that a given MS takes place. It should be noted that $p(MS)$ is characterized for stochastic ground motions (see e.g., [21]); nevertheless, it has been assumed simplistically that different records in the set of MS ground motion are equally likely to take place (see also [21, 22] for similar applications). Therefore, Eq. (4) can be approximated by the average of $P(LS_{as}|MS)$ values over the set of N MS ground-motion records which have not caused LS excursion for the intact structure. The term $P(LS_{as}|MS)$ can be estimated as follows [11] (see also the aftershock risk assessment procedure derived in [10, 19]):

$$P\left(LS_{as} \mid MS_i\right) = \sum_{n_{as}=1}^{N_{as}} P\left(LS_{as} \mid MS_i, n_{as}\right) P\left(n_{as} \mid MS_i\right) \tag{5}$$

where N_{as} be the maximum number of AS events that may take place in the time interval $[0,\tau]$; $P(LS_{as}|MS_i,n_{as})$ is the probability of exceeding the limit state LS for the first time given that exactly n_{as} aftershock events take place, and given the ith mainshock MS_i; the term $P(n_{as}|MS_i)$ is the conditional probability that exactly n_{as} aftershock events take place, and is expressed herein by a non-homogenous Poisson probability distribution:

$$P\left(n_{as} \mid MS_i\right) = \frac{\left(\nu_{as,i}\right)^{n_{as}} e^{-\nu_{as,i}}}{n_{as}!} \tag{6}$$

where $\nu_{as,i}$ is a time-decaying rate based on the Modified Omori (MO) aftershock occurrence model [23], and is equal to the number of aftershocks with magnitude between $M_{l,as} \leq M_{as} \leq M_u$ taken place in time interval $[0,\tau]$ measured with respect to the time of occurrence of the triggering MS, t_{ms}, with magnitude m_i ($\nu_{as,i}$ is both time- and MS magnitude-dependent). This aftershock occurrence rate is calculated based on MO law (see [24] for more details):

$$\nu_{as,i} = \left(10^{a+b\left(m_i - M_{l,as}\right)} - 10^{a+b\left(m_i - M_u\right)}\right) \cdot \mathrm{I}_0 \quad , \ \mathrm{I}_0 = \begin{cases} \left[\left(\tau + c\right)^{1-p} - \left(c\right)^{1-p}\right] / \left(1-p\right) & p \neq 1 \\ \ln\left[\left(\tau + c\right)/c\right] & p = 1 \end{cases} \tag{7}$$

The parameters a, b, c and p of the MO model can be derived from a generic territorial model (e.g., [25]) or can be tuned-in to a specific sequence (see e.g., [19], [24], and [25]). The probability $P(LS_{as}|MS_i,n_{as})$ in Eq. (5) can be calculated by taking into account the set of mutually exclusive and collectively exhaustive (MECE) events that *LS* first-excursion happens after one and just one of the n_{as} AS events [10, 11]:

$$P\left(LS_{as} \mid MS_i, n_{as}\right) = \sum_{k=1}^{n_{as}} \left(\Pi_{k,i} \cdot \prod_{j=1}^{k-1} \left(1 - \Pi_{j,i}\right) \right) \tag{8}$$

where $\Pi_{k,i}$ denotes the probability of *LS* first-excursion due to the occurrence of the *k*th AS event in the sequence given that the limit state has not been exceeded in the previous (*k*-1) events, and given the MS wave-form MS_i. The probability term $\Pi_{k,i}$ can be calculated as follows [10]:

$$\Pi_{k,i} = 1/\nu_{as,i} \int_{\forall sa_{as}} \pi_{k,i}\left(sa_k\right) \cdot \left| \mathrm{d}\lambda_{as,i}(sa_k) \right| \tag{9}$$

where sa_k is $Sa(T)$ associated with the *k*th aftershock event; $\pi_{k,i} = P(LS_k|sa_k, MS_i)$ is an *event-dependent* fragility for the *k*th aftershock event (defined as the probability of exceeding the limit state *LS* due to the *k*th AS event given that it has not been exceeded due to the previous (*k*-1) AS events given MS_i; $\lambda_{as,i}$ is the mean (in units of time *t*) rate of exceeding $Sa(T)$ equal to sa_{as} in time interval $[t_{MS}, t_{MS}+\tau]$ given MS wave-form MS_i (for detailed description of aftershock hazard assessment, see [24]).

The term $P(LS_{as}|MS_i)$ in Eq. (5) can also be approximated with a closed-form analytic expression (see [11] for the complete derivation of the closed=form expression). A preliminary version of this closed-form expression was proposed in [27-29]. Assume that the set of probability terms $\{\Pi_{k,i}|k=1:n_{as}\}$ for a given MS wave-form MS_i are identical and equal to the time-invariant function Π_i. Thus, the closed-form approximation to the time-dependent limit state probability $P(LS_{as}|MS_i)$ is derived as:

$$P(LS_{as} \mid MS_i) = 1 - \exp\left(-\Pi_i \nu_{as,i}\right) = 1 - \exp\left(- \int_{\forall sa_{as}} \pi_i\left(sa\right) \cdot \left| \mathbf{d}\lambda_{as,\mathrm{i}}(sa) \right| \right) \tag{10}$$

The closed-form expression in Eq. (10) has the same functional form as the expression for limit state probability exceedance in Eq. (2). However, in this case, the prediction time interval for limit state first excursion is equal to the aftershock forecasting interval $[t_{MS}, t_{MS}+\tau]$ and it is implicitly considered in the aftershock hazard term $\lambda_{as,i}$. Arguably, based on the choice of fragility term $\pi_i(sa)$ corresponding to MS_i, the closed-form derived in Eq. (10) can lead to different approximate solutions. The expression in Eq. (10) is derived by assuming that the structure is “renewed” to some invariant “average” state right after each aftershock takes place, represented by the fragility term $\pi_i(sa)$. The most obvious choice for $\pi_i(sa)$ is perhaps the fragility of the MS-damaged structure (denoted herein by $\pi_{1,i}(sa_1)$, i.e., k=1) since it is used (with some variations) by several researchers as a proxy to the aftershock vulnerability of a given structure. It is expected that the closed-form estimate to $P(LS_{as}|MS_i)$ in Eq. (10) and based on the MS-damaged fragility would capture to some extent (but not entirely) the damage accumulation potential of the sequence. Another choice for $\pi_i(sa)$ is the fragility of intact structure denoted by $\pi_0(sa_{ms})$. In this case, the closed-from approximation cannot capture the damage accumulation potential of the aftershocks. Nevertheless, and compared to conventional risk estimation considering only the strong motion, Eq. (10) has the advantage of incorporating the time-dependent aftershock hazard.

Substituting $P(LS_{as}|MS_i)$ in Eq. (10) into Eq. (4), the closed-form approximation to P_{as} can be written as:

$$\mathrm{P}_{as} \approx 1/N \sum_{MS_i} \left[1 - \exp\left(-\Pi_i \nu_{as,i}\right)\right] \tag{11}$$

This term can then be substituted in Eq. (2) in order to derive the first-excursion limit state exceedance probability in time interval [0,t].

2.1 The (time- and history-dependent) structural performance variable

The structural performance variable denoted as $Y_{LS}^{(k)}$ is adopted ([10, 11, 25]):

$$Y_{LS}^{(k)} = \frac{D_{\max}^{(k)} - D_r^{(k-1)}}{C_{LS} - D_r^{(k-1)}} \tag{12}$$

where $Y_{LS}^{(k)}$ is the critical demand to capacity ratio due to the kth event for the structure that has already been subjected to the sequence of (k-1) events; $D_{\max}^{(k)}$ is the maximum demand parameter due to the kth event; $D_r^{(k-1)}$ is the associated residual demand corresponding to the sequence of (k-1) events; C_{LS} is the limit state capacity of the (intact) structure. The performance variable $Y_{LS}^{(k)}$ tends to reflect and to conditionally isolate the effect of the kth event on the structure.

2.2 Event-dependent fragility assessment

In order to estimate the event-dependent fragility term(s) π_0 (Eq. 3) and $\pi_{k,i}$, k=1:N_{as} (see Eq. 9), a non-linear dynamic analysis procedure known as the *Modified Cloud Analysis* (MCA, [17]) is adopted (see also [11]). Herein, a sequential version of the MCA (described in a step-by-step manner in [11]) has been adopted in order to mimic the effect of back-to-back ground motion records on the structure. However, the sequential analysis procedure described and implemented in this work is an improved and version of the procedure reported in [10]: it is rendered more robust against extrapolations and it explicitly accounts for the “collapse” cases.

The event-dependent fragility assessment in [10] is performed by simple Cloud Analysis (CA, [16, 17, 30]). Although CA is a simple method to implement, it is subjected to a series of simplifying assumptions. One of these assumptions is that the conditional distribution of the structural performance variable $Y_{LS}^{(k)}$ given the intensity measure sa_k is described by a Lognormal distribution whose parameters (median and logarithmic standard deviation) are estimated by a linear regression in the logarithmic space of CA pairs (sa_k, $Y_{LS}^{(k)}$) for the kth event. Moreover, it is assumed that the conditional standard deviation in the structural performance variable given intensity is a constant (i.e., does not depend on the intensity level). Such assumption may lead to inaccurate estimates; especially in cases where the structure experiences global dynamic instability (denoted hereafter as C, manifesting itself as very high global displacement-based demands) due to a certain record or records belonging to the suite of records used for CA. This problem can be addressed by applying the standard CA only to that portion of the suite of records which does not lead to dynamic instability (denoted hereafter as NoC). The rest of the records can be treated by employing alternative methods, such as, the logistic regression (see [17] for more details on MCA). In such an approach, the event-dependent fragility term π_k (note that subscript i is dropped both for the simplicity of the formulation and also because the treatment of collapse cases is applicable to both intact and damaged structures) can be expanded as follows using MCA procedure (see [17] for the derivation of this expression):

$$\pi_k = \Phi\left(\frac{\ln \eta^{(k)}_{Y_{LS}|Sa,NoC}}{\beta^{(k)}_{Y_{LS}|Sa,NoC}}\right)\cdot\frac{e^{-(\beta_0+\beta_1\cdot\ln sa_k)}}{1+e^{-(\beta_0+\beta_1\cdot\ln sa_k)}}+\frac{1}{1+e^{-(\beta_0+\beta_1\cdot\ln sa_k)}} \tag{13}$$

where Φ is the standardized Gaussian Cumulative Density Function (CDF); $\eta_{YLS|Sa,NoC}{}^{(k)}$ and $\beta_{YLS|Sa,NoC}{}^{(k)}$ are conditional median of $Y_{LS}{}^{(k)}$ and standard deviation (dispersion) of the natural logarithm of $Y_{LS}{}^{(k)}$ for the portion of the CA suite of records that does not lead to dynamic instability cases; β_0 and β_1 are the parameters of the logistic regression model for expressing the probability of global dynamic instability. With reference to Eq. (13): (see [10, 11])

$$\ln \eta^{(k)}_{Y_{LS}|Sa,NoC}\left(sa_k\right)=\ln a_k + b_k \ln\left(sa_k\right),\ \beta^{(k)}_{Y_{LS}|Sa,NoC}=\sqrt{\frac{\sum_{m=1}^{N(k)}\left(\ln Y^{(k)}_{LS,m}-\ln a_k - b_k \ln(sa_{k,m})\right)^2}{N\left(k\right)-2}} \tag{14}$$

where $N(k)$ is the number of records for CA and is equal to $N(k)$=$N_{\text{cloud}}(k)$-$N_C(k)$; $N_{\text{cloud}}(k)$ is the number of ground motion records employed in the CA in order to represent the record-to-record variability in the kth event (the sample size for different k levels can be variable); $N_C(k)$ is the number of records that lead to the global dynamic instability (C or "collapse-cases"). The logistic regression model described in Eq. (13) is applied to all $N_{\text{cloud}}(k)$ records; they are going to be distinguished by 1 or 0 depending on whether they lead to C or NoC.

3 NUMERICAL APPLICATION

3.1 Case-study structure

The methodology described in Section 2 is applied herein in order to perform risk assessment for MS+AS sequence for a typical partially-infilled moment-resisting RC building located in L'Aquila, central Italy. The case-study structure is a shear building model representing a two-dimensional, 3-story, and 2-bay RC frame with smooth rebars. It is representative of a prevalent class of RC building structures widely constructed between 1940 and 1970 in Italy. The frame is characterized with one-bay infill panel (see Figure 2(a) for the illustration). A nonlinear shear-type building model (assuming that the building mass is lumped at the floor levels and the floor beams are rigid) is constructed in OpenSees (http://opensees.berkeley.edu). Since this model was defined previously by the authors [10, 11], important issues about the modeling and underlying assumptions are briefly described herein. Preliminary analyses on the frame revealed that the damage is mainly accumulated in the first story; hence, in order to simplify the representative mathematical model, the nonlinear behavior is attributed only to the elements located in the first level (considering a lumped plasticity model), while the upper stories are considered to remain elastic. The displacement of the first story is taken to be the corresponding engineering demand parameter herein. Figure 2(b, c) also shows the cyclic response of columns as well as infill in the first story (see also [10] for comprehensive details). For columns, the cyclic response is calibrated against the full scale test on a specimen with dimension and reinforcement details matched with the columns in the case-study structure. The parameters of the Pinching4 Material in OpenSees are chosen to closely match the real hysteretic behavior, as illustrated in Figure 2(c). On the other hand, a simple hysteretic rule with no stiffness degradation is considered for infill panel using the Hysteretic Material in Opensees library (see [10] for more discussions).

The performance objective for post-earthquake assessment of the aforementioned structure is defined in terms of the discrete limit state of Near Collapse (based on the European standard EC8 [31]). The near-collapse limit state threshold is defined with respect to the pushover analysis of the one-bay infill frame. It is conservatively set herein to 10% drop in the ultimate strength of the columns (a maximum of 20% is recommended by EC8 [30]). Figure 2(d) shows the onset of the limit state (referred to as the limit state capacity C_{LS} in Eq. 12) marked on the pushover curve by red star. The first-mode period of the building is equal to 0.27sec. To perform nonlinear dynamic analysis, a Rayleigh damping is employed with a critical damping coefficient of 5% for the first two modes of vibration. The cyclic pushover of the structure is also shown in Fig. 2(e).

It is also important to define a threshold defining the Collapse (associated with the global instability, C) of the structures. A drift ratio of 10% is taken as the threshold of indicating the "collapse" cases (as shown in Figure 2d), which corresponds herein to around 60% reduction in ultimate capacity. It is noteworthy that for concrete frame structures, a 4% drift ratio for severe damage is proposed in [32], which is consistent with the near-collapse limit state threshold herein. Consequently, adopting a 10% drift ratio for the global instability, denoted as C, somehow implies that drift demands beyond this threshold correspond to large deformation ranges.

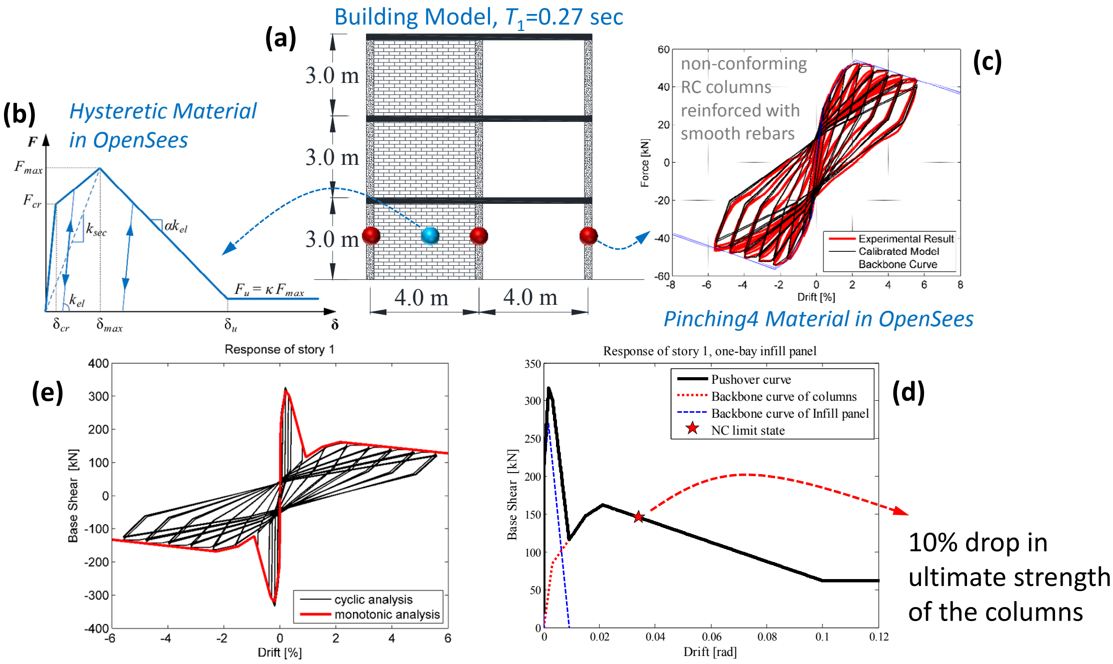

Figure 2: (a) General configuration of the case-study; (b, c) monotonic and cyclic response of columns and infill panel, (d) pushover curve in terms of the base shear versus displacement of the first story level and the points corresponding to the NC and Collapse limit states, (e) cyclic pushover of the building.

3.2 Seismic hazard assessment and ground motion selection

The reference structure is located within the central Italy, Abruzzo region, the town of L'Aquila in the seismic zone 923 based on the ZS9 Italian Seismogenetic Zonation [33]. Fig. 3(a) shows the seismogenic zonation ZS9 with different zones identified on it. The seismic hazard is estimated for the designated site (red triangle in Figure 3b) according to the surrounding seismic zones 918, 919, 920, and 923, separately indicated also in Fig. 3(b). The seismicity rate ν_{ms}=0.60, used in Eq. (2), is calculated as the sum of the seismicity of individual zones; the lower-bound magnitude M_l=4.76 for all zones, while the upper-bound magnitude M_u varies from 6.14 (Z920) up to 7.06 (Z923). Based on the seismicity data of each zone, a simplified site-specific probabilistic seismic hazard analysis (PSHA) is performed on the desired site. The Sabetta and Pugliese attenuation relation (SP96, [34]) is chosen because of its wide use in Italy.

The aftershock hazard is calculated by integrating the adopted ground-motion prediction equation over all possible aftershock magnitudes and distances within the desired aftershock zone (see [19, 24, 35] for more details). The aftershock zone considered herein is the one presented in [10, 24], which is indicated as ZAS with cyan color in Figure 3(b). The aftershock magnitudes are within the range of $4.0 \leq M_{as} \leq 7.06$. The occurrence of aftershocks is modeled by the MO model with the parameter estimated for the Italian generic aftershock sequence based on aftershock events occurring from 1981 to 1996 [26]. Figures 3(c) shows the comparison between seismic hazard considering only MS (long-term seismic hazard λ_{ms}) and the short-term seismic hazard associated with triggered aftershock events ($\lambda_{as,i}$ for τ=1 day, and MS number i=14).

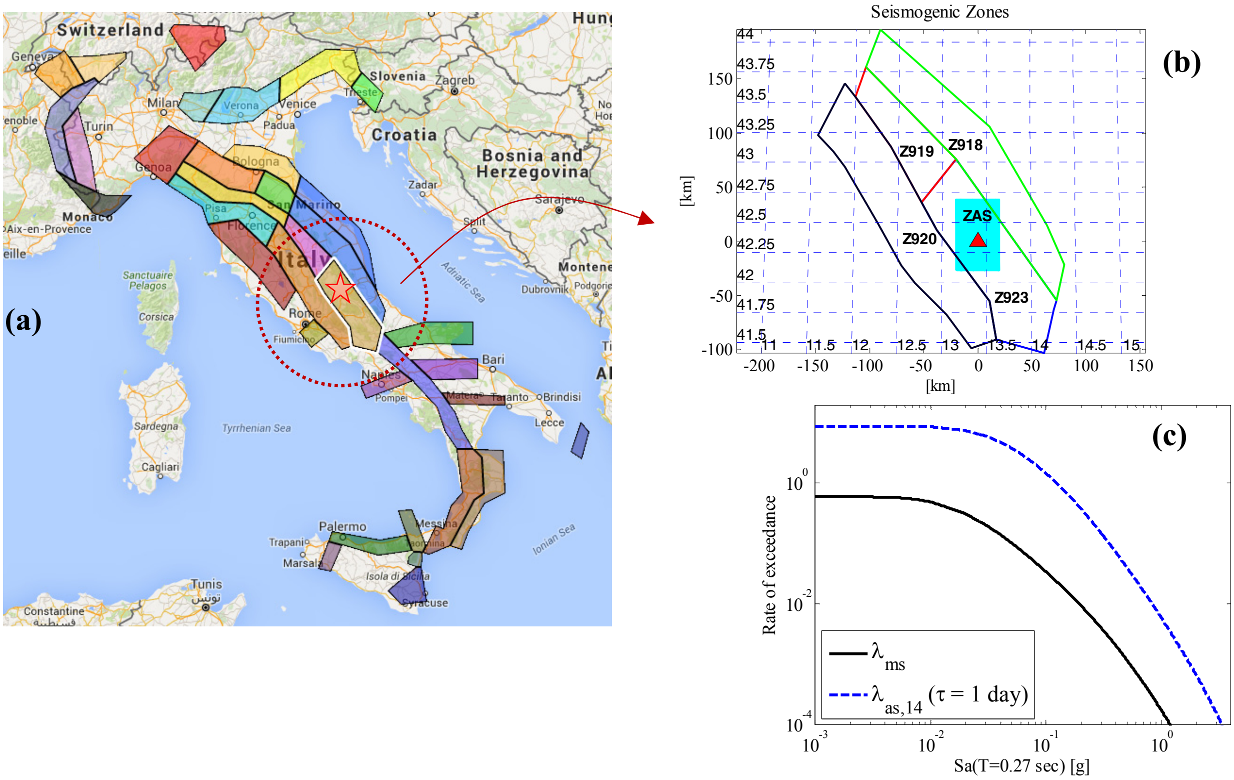

Figure 3: (a) The Italian seismogenic zonation and the site of interest indicated by a pentagram, (b) the four seismogenic zones surrounding the case-study site (defined by red triangle), and the aftershock zone (ZAS) with cyan color, (c) site-specific seismic hazard

A set of 50 European (especially Italian) strong ground motion (MS) records are selected from the NGA-West2 database [36], and listed in [11]. This suite of records covers a wide range of magnitudes between 5.50 and 7.50, and closest distance to ruptured area (R_{RUP}) up to around 80 km. AS record set consists of a set of 43 European (especially Italian) aftershock ground-motion records selected based on the classification of the NGA-West2 database for aftershock records [36], and listed in [11]. This suite of selected records covers the range of low magnitudes between 4.20 and 6.20, and R_{RUP} up to around 40 km. Both set of ground motions are chosen without emphasizing on detailed record selection.

3.3 Step-by-step procedure for time-dependent risk calculation

To estimate the event-dependent fragilities and the time-dependent limit state probabilities, the sequential MCA is applied herein. While the procedure described in [10] was specifically targeted to MS-damaged structures (conditioned on knowing the MS wave-form), the modified version described herein can be applied to risk assessment in general considering the effect of aftershocks. A step=by-step procedure is described as follows:

Step (1): A suite of ground-motion records is selected from the pool of MS strong-motion recordings which represent the MS records. The fragility of the intact structure, π_0, (Level 0) is calculated by adopting the MCA. In the next step, P_{ms} is calculated from Eq. (3). Figure 4(a) illustrates the Cloud regressions and the associated MS-induced fragility curves, π_0, for the case-study frame using the set of strong motion (MS) records outlined in [11]. For each scatter Cloud data (colored squares), the corresponding record ID is shown. The red-colored squares indicate the collapse-cases, C. The line Y_{LS}=1 showing the onset of near-collapse limit state excursion is also indicated on this figure. The fragility curve is calculated by using the expression in Eq. (13) considering the collapse-cases explicitly and plotted as thick black lines. They are compared with the fragility curves calculated from CA considering only the non-collapse cases (dashed lines, see [10, 11]). It can be seen that the explicit consideration of collapse-cases in MCA leads to a slight difference (the fragility shifts to the left which means that the structure becomes more vulnerable).

Step (2): The selected suite of MS ground motions is partitioned into two mutually exclusive subsets: those which cause the structure to exceed the limit state (herein, Near Collapse), and the rest of the records that do not lead to limit state excursion. It should be noted that the ground motion records that cause C (collapse-cases) are a subset of records that cause limit state excursion.

Step (3): Each one of the records that does not lead to limit state excursion is followed (in a back-to-back manner) with a suite $N_{\text{cloud}}(1)$ of records (i.e., $N_{\text{cloud}}(1)$ sequences of MS-AS) consisted of AS recordings (selected from the pool of aftershock records) plus those mainshock records that have led to limit state excursion in Step 2. The latter set of records has been included in order to ensure that the Cloud response has few data points with (Y>1), so that no extrapolation is necessary. The MS records that have led to limit state excursion are only used for ensuring that the Cloud procedure has enough data points associated with Y>1. Note that these records are not going to be used for constructing an (ongoing) AS sequence. This is because any seismic sequence that has one of this records in Level 1 or higher is going to be automatically interrupted (i.e., a record that has caused the intact structure to exceed the limit state is definitely going to lead the damaged structure to exceed the same limit state). This is an effective way of making sure that the CA results are reliable (avoid extrapolations). By adopting MCA, the fragility of MS-damaged structure conditioned on a given MS wave-form MS_i (a.k.a. the event-dependent fragility $\pi_{1,i}$, Level 1) is calculated (see Fig. 4b; note that the CA and the associated event-dependent fragilities in Fig. 4 correspond to MS_{20} presented in [11]). The procedure leads to estimating $\Pi_{1,i}$ from Eq. (9) by integrating the MS-damaged fragility and aftershock hazard.

Step (4): In the next step, the MS-AS sequences that have not led to limit state exceedance are going to be expanded into $N_{\text{cloud}}(2)$ MS-AS-AS sequences (by appending a ground motion record in a back-to-back manner). The AS records are in part permutated from the suite of AS recordings described in Step (3), and in part from the MS records that have led to limit state excursion defined in Step (2). The event-dependent fragility $\pi_{2,i}$, (Level 2) conditioned on a given MS waveform MS_i, is calculated by adopting the MCA (see Fig. 4c). As a result, $\Pi_{2,i}$ can be again calculated from Eq. (9).

Step (5): Step 4 is going to be repeated until there is at least one Y-value smaller than 1. Following this step, the event-dependent fragility $\pi_{k,i}$, conditioned on a given MS waveform MS_i, is calculated by adopting the MCA (see e.g., Fig. 4d for $\pi_{3,20}$, Level 3).

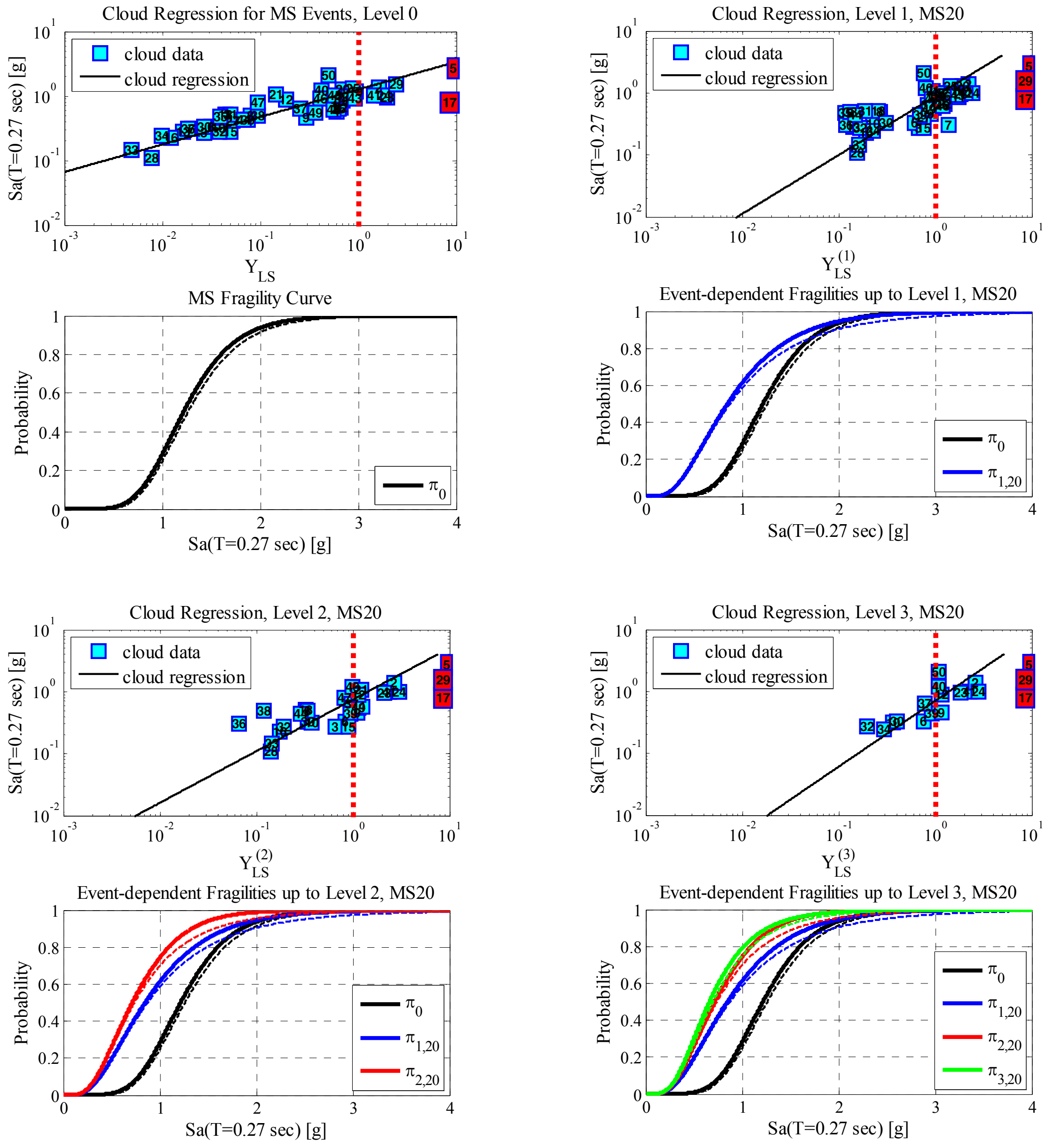

Figure 4: The schematic diagram of the sequential MCA procedure, (a) Calculation of the fragility of intact structure, π_0; (b, c, d) the event-dependent fragilities $\pi_{1,20}$ up to $\pi_{3,20}$ (given MS_{20}) for the case-study structure; the AS sequence is constructed based on back-to-back records from the MS record set

Step (6): The event-dependent limit state probabilities $\Pi_{k,i}$, k=1:N_{as}, (estimated through Steps 1-5) are going to be employed in order to calculate the probability $P(LS_{as}|MS_i,n_{as})$ from Eq. (8).

Note: The limit state probability $P(LS_{as}|MS_i,n_{as})$ (due to aftershocks) given the MS_i waveform and n_{as} can be calculated from the recursive formulation in Eq. (8) as a function of $\{\Pi_{k,i}|k=1:N_{as}\}$. Calculating $\Pi_{k,i}$ by using Eq. (9) leads to the "*best-estimate*" limit state excursion probability due to the aftershocks $P_{as}(\tau)$. However, we propose three alternative approximations based on the closed-form approximation derived in Eq. (11) by setting:

(a) $\Pi_i = \Pi_0$ (the fragility of the intact structure)

(b) $\Pi_i = \Pi_{1,i}$ (the fragility of the MS-damaged structure given MS_i)

(c) $\Pi_i = \Pi_{2,i}$ (the fragility of the MS-plus-one-AS-damaged structure given MS_i)

Step (7): The limit state probability $P(LS_{as}|MS_i)$ denoting the probability of exceeding the limit state LS for the first time given MS_i is calculated from Eq. (5). With reference to Eq. (5), the conditional probability of having exactly n_{as} aftershock events, $P(n_{as}|MS_i)$, is estimated by the Poisson probability distribution from Eq. (6).

Step (8): The $P(LS_{as}|MS_i)$ values, calculated for each of the MS waveforms that did not lead to limit state excursion in Step (2), are averaged according to Eq. (4) in order to approximate the probability that the first limit state excursion is due AS sequence, P_{as}. Figure 5(a) and 5(b) depict the quantities $P_{as}(\tau)$ and P_{ms} as a function of the aftershock forecasting time window τ elapsed after the MS, where the AS sequence is assembled from the pool of MS records and from the pool of AS records (see [11] for the set of MS and AS records).

Step (9): The P_{as} (from Step 8) and P_{ms} (from Step 1) are substituted in Eq. (2) in order to calculate the probability of exceeding the limit state in time interval $[0,t]$ taking into account also the effect of aftershocks. Figures 5(c) and 5(d) plot the limit state excursion probabilities $P(LS)$ in Eq. (2) in time interval $[0,t]$ for a fixed value of aftershock forecasting interval τ=7 day, where the AS sequence is constructed based on the two distinct MS and AS sets of records, respectively.

3.4 Discussion on the Results

In Figure 5(a) and 5(b), slight difference can be noticed in the results obtained based on the two different pools of records. This confirms that construction of AS sequence by back-to-back positioning of strong-motion records might cause overestimation in P_{as} (this is also observed in previous research efforts, see e.g. [5-8]). Nevertheless, this overestimation is not highly significant herein. Next, it can be observed that taking into account the effect of triggered aftershocks (the "*best-estimate*" represented by the thick black line) changes the limit state probability significantly, as compared with a "classical" risk assessment due to mainshocks only (i.e., P_{ms} represented by dotted red line). In addition, the approximate solution based on $\Pi_i = \Pi_0$ (plotted as dashed-dot cyan line) leads to significantly higher estimates for $P_{as}(\tau)$ with respect to P_{ms}, although it does not consider the damage accumulation due to the aftershock sequence. The reason is that this approximate solution considers the increased short-term seismicity due to the aftershock sequence. The approximate solution based on $\Pi_i=\Pi_{1,i}$ and plotted as dashed blue line, that partially manages to capture the damage accumulation due to aftershocks, leads to $P_{as}(\tau)$ estimates closer to those obtained based on the *"best-estimate"* procedure. Finally, the approximate solution based on $\Pi_i=\Pi_{2,i}$ and plotted as grey thick line, manages to provides estimates for $P_{as}(\tau)$ still closer to those provided by the *"best-estimate"* procedure.

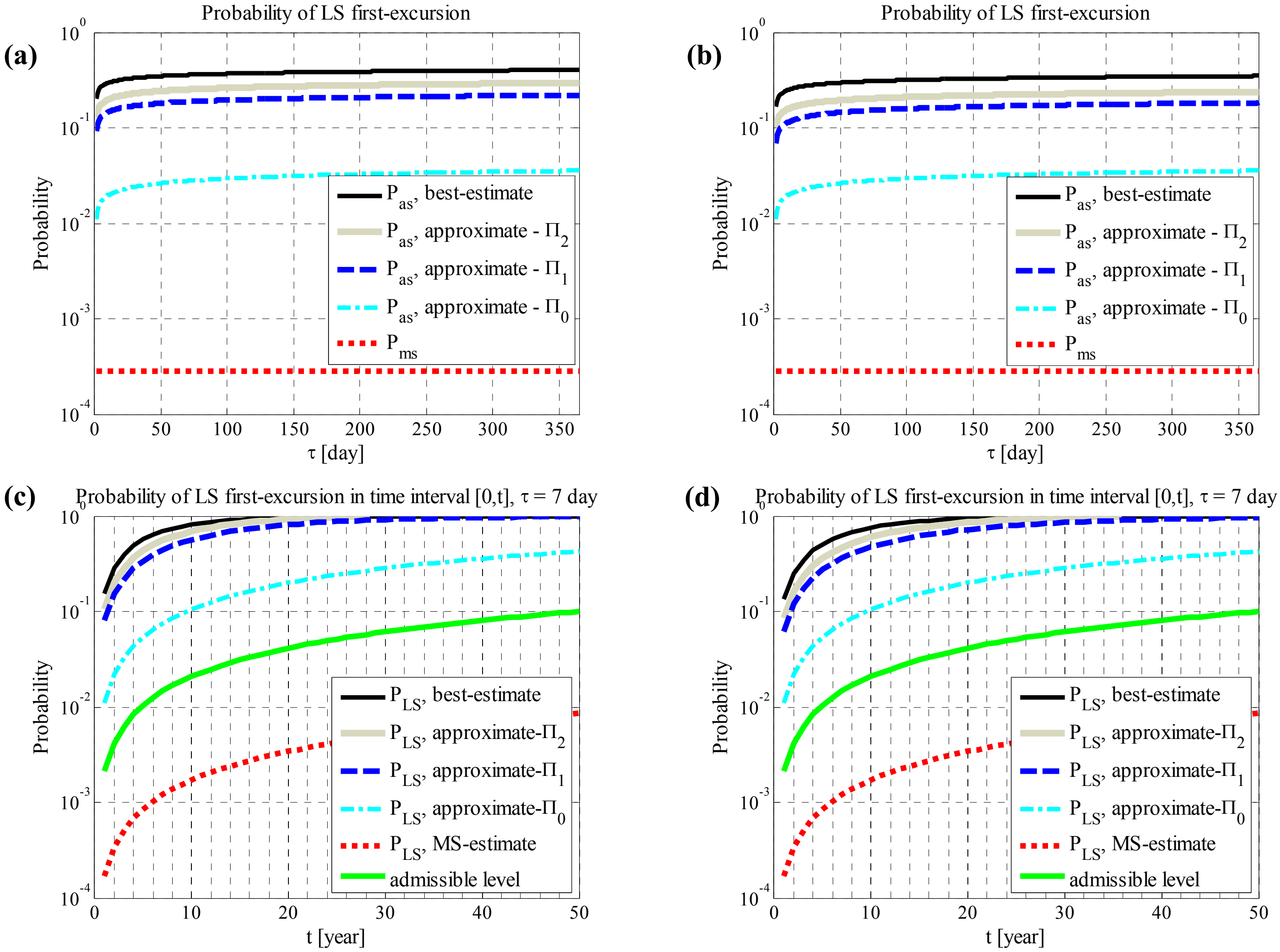

Figure 5: Comparison between different risk-related metrics by considering only MS and the MS+AS sequence when the AS sequence is generated from (a, c) the MS record set, (b, d) the AS record set; τ is the forecasting window for the triggered aftershocks, and $[0,t]$ is the temporal interval for *LS* exceedance

Figures 5(c) and 5(d) plot the limit state excursion probabilities $P(LS)$ in Eq. (2) in time interval $[0,t]$ for a fixed value of aftershock forecasting interval τ=7 day, where the AS sequence is constructed based on the two distinct MS and AS sets of records, respectively. It can be observed that the approximation based on $\Pi_i=\Pi_{1,i}$ (MS-damaged structural fragilities, dashed blue line) does not manage to fully capture the cumulative damage due to the aftershock sequence, although it provides a very good partial estimate. To a much lesser extent, the approximation based on $\Pi_i=\Pi_0$ (i.e., intact structural fragility, dashed-dot cyan) manages to follow the trend in the limit state probability due to the MS and the triggered AS sequence. Although this approximation does not capture the damage accumulation, it manages to take into account the (time-dependent) increase in short-term seismicity due to the triggered aftershock sequence. The solution based on $\Pi_i=\Pi_{2,i}$ (MS-plus-one-AS-damaged structural fragility, thick grey line) seems to provide an excellent balance between reduced analysis effort (a maximum of three back-to-back events are considered) and accuracy (close match with *"best-*

estimate" results). These plots also feature the admissible limit state probability level (plotted as a thick green line) taken to be equal to 1-$e^{(-0.0021t)}$ (associated with 10% exceedance probability in 50 years). It can be seen that the limit state probability calculated by considering the mainshocks only (plotted as a dotted red-line) is below the admissible level; however, considering the triggered AS sequence (in the *"best-estimate"* procedure and the three alternative approximations) leads to risk levels that exceed the admissible level. As before, it is observed that the results are sensitive to the selected pool of ground motion records for construction of AS sequence.

4 CONCLUSIONS

- The classical risk assessment based on strong ground-motion (only MS) cannot consider the effect of triggered aftershocks and –under certain conditions– may lead to significant underestimation. In order to consider the sequence of aftershocks in seismic risk assessment, both the increase in short-term seismicity and the potential for damage accumulation should be considered.
- The simplified (closed-form) solution proposed herein with the fragility of intact structure is somehow equivalent to considering the short-term increase in seismicity, without considering the effect of cumulative damage.
- Using the closed-form solution with the MS-damaged fragility manages to consider the short-term increase in seismicity as well as the effect of cumulative damage as some sort of a first-order approximation. The risk estimate improves with respect to MS-only and closed-form based on intact fragility results. However, it still underestimates the risk when compared to the best-estimate results.
- The proposed methodology is implemented using a non-linear dynamic analysis routine known as the Modified Cloud Analysis (MCA). The sequential MCA methodology presented herein, compared to the earlier version presented in [10], has two significant advantages. First, it adopts a simple but effective technique in order to make sure that performance assessment based on the Cloud Analysis procedure avoids extrapolations; second, it can explicitly account for the "collapse" cases where the structure experiences global dynamic instability (i.e., very large global displacement-based demands).

AKNOWLEDGEMENT

This work is supported in part by the Project METROPOLIS (Metodologie e Tecnologie Integrate e Sostenibili Per L'adattamento e La Sicurezza di Sistemi Urbani). This supports is gratefully acknowledged.

REFERENCES

[1] P. Bazzurro P, C.A. Cornell, C. Menun, N. Luco, M. Motahari, *Advanced seismic assessment guidelines*. Pacific Earthquake Engineering Research Center (PEER), 2004/03.

[2] N. Luco, P. Bazzurro, C.A. Cornell, Dynamic versus static computation of the residual capacity of mainshock-damaged building to withstand an aftershock. *13th World Conference on Earthquake Engineering*, Vancouver, B.C., Canada, August 1-6, 2004.

[3] M. Raghunandan, A.B. Liel, N. Luco. Aftershock collapse vulnerability assessment of reinforced concrete frame structures. *Earthquake Engineering and Structural Dynamics*, **44** (3), 419-439, 2015

[4] G.L. Yeo, C.A. Cornell. Equivalent constant rates for post-quake seismic decision making. *Structural Safety*, **31** (5), 443-447, 2009

[5] Q. Li, B.R. Ellingwood, Performance evaluation and damage assessment of steel frame buildings under main shock-aftershock sequences. *Earthquake Engineering and Structural Dynamics*, **36** (3), 405-427, 2007.

[6] K. Goda. Record selection for aftershock incremental dynamic analysis. *Earthquake Engineering and Structural Dynamics*, **44** (7), 1157-1162, 2015.

[7] S. Tesfamariam, K. Goda, Loss estimation for non-ductile reinforced concrete building in Victoria, British Columbia, Canada: effects of mega-thrust Mw9-class subduction earthquakes and aftershocks. *Earthquake Engineering and Structural Dynamics*, **44** (13), 2303-2320, 2015.

[8] J. Ruiz-García, J.C. Negrete-Manriquez. Evaluation of drift demands in existing steel frames under as-recorded far-field and near-fault mainshock–aftershock seismic sequences. *Engineering Structures*, **33** (2), 621-634, 2011

[9] A. Faisal, T.A. Majid, G.D. Hatzigeorgiou, Investigation of story ductility demands of inelastic concrete frames subjected to repeated earthquakes. *Soil Dynamics and Earthquake Engineering*, **44**, 42-53, 2013.

[10] H. Ebrahimian, F. Jalayer, D. Asprone, A.M. Lombardi, W. Marzocchi, A. Prota, G. Manfredi, A performance-based framework for adaptive seismic aftershock risk assessment. *Earthquake Engineering and Structural Dynamics*, **43** (14), 2179-2197, 2014.

[11] F. Jalayer, H. Ebrahimian, Seismic risk assessment considering cumulative damage due to aftershocks. *Earthquake Engineering and Structural Dynamics*, **46** (3), 369–389, 2017.

[12] K. Goda, C.A. Taylor, Effects of aftershocks on peak ductility demand due to strong ground motion records from shallow crustal earthquakes. *Earthquake Engineering and Structural Dynamics*, **41** (15), 2311-2330, 2014

[13] G.D. Hatzigeorgiou, D.E. Beskos. Inelastic displacement ratios for SDOF structures subjected to repeated earthquakes. *Engineering Structures*, **31** (11), 2744-2755, 2009.

[14] D. Vamvatsikos, C.A. Cornell. Incremental dynamic analysis. *Earthquake Engineering and Structural Dynamics*, **31** (3), 491-514, 2002.

[15] M. Gaetani d'Aragona, M. Polese, K.J. Elwood, M. Baradaran Shoraka, A. Prota, Aftershock collapse fragility curves for non-ductile RC buildings: a scenario-based assessment. *Earthquake Engineering & Structural Dynamics*, **46**(13), 2083-2102, 2017.

[16] F. Jalayer, R. De Risi, G. Manfredi, Bayesian Cloud Analysis: efficient structural fragility assessment using linear regression. *Bulletin of Earthquake Engineering* **13**(4), 1183–1203, 2015.

[17] F. Jalayer, H. Ebrahimian, A. Miano, G. Manfredi, H. Sezen, Analytical fragility assessment using unscaled ground motion records. *Earthquake Engineering and Structural Dynamics* **46**(15), 2639–2663, 2018

[18] A. Miano, F. Jalayer, H. Ebrahimian, A. Prota, Cloud to IDA: Efficient fragility assessment with limited scaling. *Earthquake Engineering and Structural Dynamics* **47** (5), 1124–1147, 2018.

[19] F. Jalayer, D. Asprone, A. Prota, G. Manfredi, A decision support system for post-earthquake reliability assessment of structures subjected to aftershocks: an application to L'Aquila earthquake, 2009. *Bulletin of Earthquake Engineering*, **9** (4), 997-1014, 2011.

[20] F. Jalayer F, Asprone D, Prota A, Manfredi G. Multi-hazard upgrade decision making for critical infrastructure based on life-cycle cost criteria. *Earthquake Engineering and Structural Dynamics*, **40** (10), 1163-1179, 2011

[21] F. Jalayer, J. Beck, F. Zareian. Analyzing the sufficiency of alternative scalar and vector intensity measures of ground shaking based on information theory. *Journal of Engineering Mechanics*, **138** (3), 307-316, 2012.

[22] H. Ebrahimian, F. Jalayer, A. Lucchini, F. Mollaioli, G. Manfredi. Preliminary ranking of alternative scalar and vector intensity measures of ground shaking. *Bulletin of Earthquake Engineering*, **13** (10), 2805-2840, 2015.

[23] T. Utsu. A statistical study of the occurrence of aftershocks. *Geophysical Magazine*, **30**, 521-605, 1961.

[24] H. Ebrahimian, F. Jalayer, D. Asprone, A.M. Lombardi, W. Marzocchi, A. Prota, G. Manfredi. Adaptive Daily Forecasting of Seismic Aftershock Hazard. *Bulletin of Seismological Society of America*, **104** (1),145-161, 2014.

[25] H. Ebrahimian, F. Jalayer, D. Asprone, A.M. Lombardi, W. Marzocchi, A. Prota, G. Manfredi. An outlook into time-dependent aftershock vulnerability assessment. *4th ECCOMAS Thematic Conference on Computational Methods in Structural Dynamics and Earthquake Engineering (COMPDYN2013)*, M. Papadrakakis, V. Papadopoulos, V. Plevris (eds.), Kos Island, Greece, 12-14 June, 2013.

[26] B. Lolli, P. Gasperini. Aftershocks hazard in Italy part I: estimation of time-magnitude distribution model parameters and computation of probabilities of occurrence. *Journal of Seismology*, **7** (2), 235-257, 2003.

[27] F. Jalayer, H. Ebrahimian, D. Asprone, A. Prota, G. Manfredi. A closed-from approximation to adaptive structural fragility to aftershocks. *10th National Conference in Earthquake Engineering*, Earthquake Engineering Research Institute, Anchorage, AK, July 21-25, 2014; paper 1649.

[28] F. Jalayer, H. Ebrahimian, G. Manfredi. Towards quantifying the effect of aftershocks in seismic risk assessment. *12th International Conference on Applications of Statistics and Probability in Civil Engineering (ICASP12)*, Vancouver, Canada, July 12-15, 2015.

[29] H. Ebrahimian, F. Jalayer, G. Manfredi. Seismic retrofit decision-making of bridges based on life-cycle cost criteria. *5th ECCOMAS Thematic Conference on Computational Methods in Structural Dynamics and Earthquake Engineering (COMPDYN 2015)*, M. Papadrakakis, V. Papadopoulos, V. Plevris (eds.), Crete Island, Greece, 25-27 May 2015.

[30] C.A. Cornell, F. Jalayer, R.O. Hamburger, D.A. Foutch. Probabilistic basis for 2000 SAC federal emergency management agency steel moment frame guidelines. *Journal of structural engineering*, **128** (4), 526–533, 2002.

[31] CEN. *Eurocode 8: design of structures for earthquake resistance*. Part 1: General rules, seismic actions and rules for buildings. EN 1998-1 CEN Brussels: April 2004.

[32] ASCE/SEI Seismic Rehabilitation Standards Committee. *Seismic Rehabilitation of Existing Buildings (ASCE/SEI 41-06)*. American Society of Civil Engineers, Reston, VA, 2007.

[33] Gruppo di Lavoro. *Redazione della mappa di pericolosità sismica prevista dall'Ordinanza PCM 3274 del 20 marzo 2003*. Rapporto Conclusivo per il Dipartimento della Protezione Civile, INGV, Milano-Roma, April 2004: 65 pp. + 5 appendixes (in Italian).

[34] Sabetta F, Pugliese A. Estimation of response spectra and simulation of nonstationary earthquake ground motions. *Bulletin of Seismological Society of America*, **86** (2): 337-352, 1996.

[35] H. Ebrahimian, F. Jalayer. Robust seismicity forecasting based on Bayesian parameter estimation for epidemiological spatio-temporal aftershock clustering models. *Scientific Reports, Nature*, **7**(9803), 1-15, 2017.

[36] T.D. Ancheta et al. NGA-West2 Database. *Earthquake Spectra*, **30** (3), 989-1005, 2014.